Journal of Alloys and Compounds 729 (2017) 171–179

Contents lists available at ScienceDirect

Journal of Alloys and Compounds

journal homepage: http://www.elsevier.com/locate/jalcom

In-situ synthesis of co-continuous aluminum-aluminum nitride composites by arc plasma induced accelerated displacement reaction

J.I. Lee [a, b], E.S. Park [a, *]

[a] Research Institute of Advanced Materials, Department of Materials Science and Engineering, Seoul National University, 1 Gwanak-ro, Gwanak-gu, Seoul, 08826, South Korea
[b] International Center for Young Scientists, National Institute for Materials Science (NIMS), 1-2-1 Sengen, Tsukuba, Ibaraki 305-0047, Japan

ARTICLE INFO

Article history:
Received 10 July 2017
Received in revised form
14 September 2017
Accepted 15 September 2017
Available online 18 September 2017

Keywords:
Metal matrix composites
Liquid-solid reaction
Microstructure
Thermal expansion
Thermal analysis

ABSTRACT

We investigate in-situ formation of co-continuous aluminum (Al)-aluminum nitride (AlN) composites with attractive mechanical and thermal properties by newly developed arc plasma-induced accelerated displacement reaction (APADR). The core innovation of the process is that it combines a simple pressureless infiltration with a thermodynamically favorable displacement reaction of silicon nitride (Si_3N_4) and molten Al under arc-plasma induced ultra-high temperature. The fast volume displacement nitridation via APADR resulted from improved wettability and enhanced diffusion of dissolved nitrogen. Thus, within a minute of APADR, Al matrix composites (AMCs) containing AlN over 50 vol% were successfully fabricated by the infiltration of Al melt into Si_3N_4 particulate preforms with different particle size distributions. The microstructures of the composites exhibited co-continuous three-dimensional network structures with strong interfacial bonding and high interfacial thermal conductance, which resulted in a unique combination of relatively high flexural strength and high thermal conductivity. In particular, the AMCs containing nitrides of 73 vol% exhibited a low coefficient of thermal expansion, close to that of GaAs or GaN used for high-power semiconductor devices, which is the lowest value ever reported among the nitride reinforced AMCs. These results would give us a promising strategy for in-situ processing routes to fabricate continuous nitride reinforced AMCs with high dimensional and mechanical stability for heat spreader applications.

1. Introduction

Al matrix composites (AMCs) have been widely used in the fields such as ground transportation, electronic packaging, aerospace and infrastructure industries [1–5]. Among them, the base materials for electronic packaging, i.e., heat spreaders, require conflicting thermal properties such as high thermal conductivity (TC) and low coefficient of thermal expansion (CTE) at the same time. To solve this problem, various AMCs with high volume fraction of ceramic reinforcements (≥50 vol%) have been developed by several processing techniques such as powder metallurgy [6], centrifugal casting [7] or pressure infiltration [8]. However, it is very difficult to form those AMCs by a simple and economical way while preventing interfacial reactions [3–5].

Aluminum nitride (AlN) has received significant attention as a second phase for the AMCs due to its thermodynamic compatibility with Al, high modulus, high TC and low CTE [9–18]. Although AMCs containing 60–85 vol% AlN could be fabricated by spark plasma sintering [9,10] or infiltration process [11], the processes require a significant external pressure up to 300 MPa due to the poor wettability between molten Al and AlN [19]. Thus, extensive studies have been focused on the fabrication of AlN reinforced AMCs with high volume fraction of AlN by in-situ processing routes that are advantageous for strong interfacial bonding between the constituents [3,4]. For example, directed melt nitridation process offers co-continuous AMCs with varying metal/ceramic ratios by treating a molten alloy in a static/flowing nitrogen gas atmosphere [16], and gas bubbling method yields particulate AMCs containing relatively large amount of AlN when ammonia gas is injected into Al melt [17,18]. However, both processes require several hours for the nitridation of Al melt at elevated temperatures higher than 1273 K, which is time-consuming and economically unfavorable. Another example is a displacement reaction that is carried out by immersing a ceramic precursor in a molten alloy where the precursor is

* Corresponding author.
E-mail address: espark@snu.ac.kr (E.S. Park).

http://dx.doi.org/10.1016/j.jallcom.2017.09.159
0925-8388/

transformed into a thermodynamically more stable phase [20–23]. According to the standard Gibb's free energies of formation for nitrides [Fig. 1(a)], the formation of AlN is favorable by the displacement reaction between molten Al and technical ceramics like silicon nitride (Si_3N_4) as follows [24]:

$$2Al_{(l)} + 1/2Si_3N_{4(s)} \rightarrow 2AlN_{(s)} + 3/2[Si]_{Al},\ \Delta H_f^{\circ} = -293\ \text{kJ/mol at } T = 1500\ K \quad (1)$$

where Si diffuses out of Si_3N_4 during the reaction and dissolves in the Al melt. While the AlN formation in Equation (1) has been reported by several works [25–28], there has been little attention paid to fabricate AlN reinforced AMCs with the displacement reaction of molten Al and Si_3N_4. The reason is that a Si_3N_4 substrate exhibits non-wetting contact angles, $\theta > 90^{\circ}$ with a drop of molten Al below 1273 K [Fig. 1(b)] [28,29]. The poor wettability of Si_3N_4 and molten Al is responsible for weak adhesion, which confines the displacement reaction between them. The contact angles decrease with the addition of alloying elements like Mg in Al [29], but Mg addition results in deleterious effects on the TC of AMCs [30]. Thus, it is essential to increase the processing temperature higher than 1273 K where molten Al wets Si_3N_4 and the displacement reaction given by Equation (1) favorably takes place.

In this study, we investigate in-situ synthesis of continuous AlN reinforced AMCs through newly developed arc plasma-induced accelerated displacement reaction (APADR). Within a minute by APADR process, the AMCs with 55 and 73 vol% nitrides were fabricated by the fast volume displacement nitridation through pressureless infiltration of Al melt into Si_3N_4 particulate preforms with different particle size distributions. The distinctive co-continuous microstructure and resultant properties such as flexural strength, CTE, and TC were systematically characterized. In particular, the AlN formation mechanism and microstructure change depending on Si_3N_4 particulate preforms in newly developed APADR process were carefully discussed.

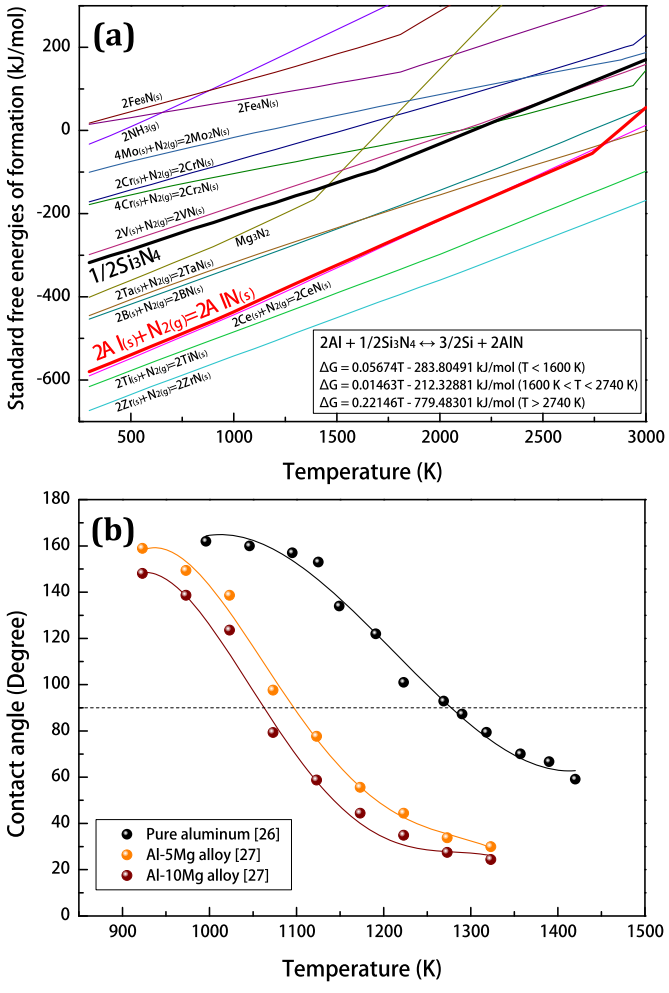

Fig. 1. (a) Standard Gibb's free energies of formation for nitrides [24] and (b) variation of contact angles between molten alloys and Si_3N_4 substrate as a function of temperature [28,29].

2. Experimental

Si_3N_4 particulate preforms were prepared by cold pressing Si_3N_4 powder with median diameter (D_{50}, the diameter of particle at 50% in the cumulative particle size distribution) of 0.7 μm (UBE industries, Tokyo, Japan) and 14.8 μm (LTS research laboratories, Orangeburg, NY, USA, −325 mesh). The size distribution of the powder was measured by a particle size analyzer (Microtrac MT3000, Nikkiso, Tokyo, Japan). Disk-shaped preforms with diameter of 13 mm and height of 2 mm were prepared by compacting the powder in a steel die and cold isostatic pressing at a global pressure of 200 MPa. The preforms were then dried in an oven at 423 K for 12 h to remove moisture. Preforms with two different particle size distributions were prepared; (a) unimodal particle size distribution (UPSD) consisting of relatively fine particles (D_{50} = 0.7 μm), and (b) bimodal particle size distribution (BPSD) consisting of coarse (D_{50} = 14.8 μm) and fine (D_{50} = 0.7 μm) particles with 7: 3 vol ratio [31]. Green density of these preforms was calculated from the sample weight and geometric dimensions, which were 45 vol% and 65 vol%, respectively.

The APADR process was carried out by arc melting with a constant arc voltage of 20 V and arc current of 150 A. First, a button-shaped Al ingot was prepared by arc melting pure Al pieces (99.999% purity) under a Ti-gettered Ar atmosphere (99.999% purity, total pressure of 40 kPa), and then the ingot, placed on a Si_3N_4 preform, was arc melted [Fig. 2(a)]. The preform was covered and reacted with molten Al, leaving a reaction layer at the rim of the preform [Fig. 2(b)]. After the as-melted Al–Si_3N_4 ingot was turned over, the ingot was arc-melted again for a minute [Fig. 2(c)]. It should be noted that the distance between tungsten electrode and the ingot was kept larger than 2 mm and arc plasma was generated on the periphery of the ingot to avoid the collapse of the preform. Within a minute of the arc melting, the preform was immersed and completely infiltrated with the Al melt, leaving disk-shaped AMCs embedded in the Al ingot [Fig. 2(d)]. During the infiltration, a small amount of Al was evaporated due to the arc plasma-induced ultra-high temperature over 2000 K (measured by pyrometer [32] and inferred from the evaporation of Al (boiling point: 2743 K)) and the exothermic heat of reaction in Equation (1). It should be noted that the displacement reaction of the dissociated N from Si_3N_4 to AlN is instantaneous due to the absence of activation energy for chemisorption. Furthermore, solubility of N in Al at 2000 K was estimated to be about 0.3 at.% [13], indicating that dissolution of the dissociated N is thermodynamically favorable. Thus, the arc melting method can be an effective route to dissolve significant amount of N into Al melt and improve wettability, and AlN can be explosively in situ formed by displacement reaction, which leads to fast volume nitridation of Al. The resultant composites fabricated by reaction of the UPSD and BPSD preforms will be denoted as UPSD and BPSD composite, respectively.

Phase constitution of the resulting composites was characterized by X-ray diffraction (XRD; New D8 Advance, Bruker, Karlsruhe, Germany) using monochromatic Cu Kα radiation for a 2θ range of

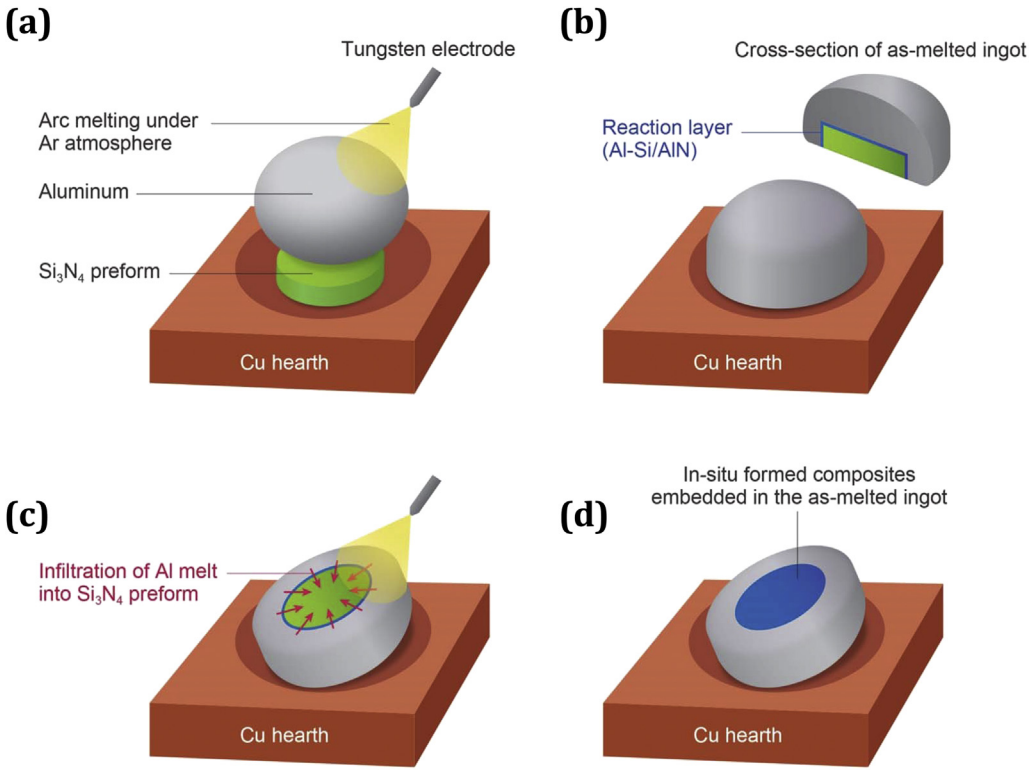

Fig. 2. Schematic diagram showing processing procedure for the fabrication of nitride reinforced co-continuous AMCs via APADR process.

20–80°. Microstructures were examined by optical microscope (OM; Eclipse LV 150, Nikon, Tokyo, Japan) and scanning electron microscope (SEM; SU70, Hitachi, Tokyo, Japan) equipped with energy-dispersive X-ray spectroscopy. Volume fraction of the second phases was evaluated from OM and SEM images using image analysis software (IMT iSolution DT version 10.3, IMT i-Solutions Inc., Vancouver, BC, Canada). Flexural strength was measured by three-point bending test with sample dimensions of $2 \times 2 \times 10$ mm. Thermal expansion behavior of the composites was characterized by thermo-mechanical analyzer (Q400, TA Instruments, New Castle, DE, USA) at a heating rate of 5 K/min with sample dimensions of $2.0 \times 2.0 \times 10$ mm. Thermal diffusivity was measured by laser flash analysis (LFA 457, Netzsch, Selb, Germany) with sample diameter of 10 mm and thickness of 2 mm in a flowing Ar atmosphere. Specific heat was determined by using differential scanning calorimetry (DSC 8500, Perkin Elmer, Waltham, MA, USA) with a heating rate of 10 K/min, and density was measured by Archimedes' method using an electrical balance (XS 204, Mettler Toledo, Greifensee, Switzerland). Thermal conductivity was calculated as a product of the measured thermal diffusivity, specific heat and density.

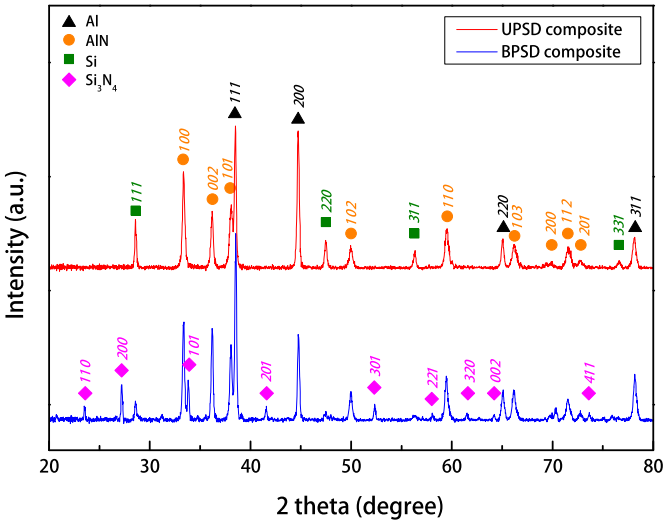

Fig. 3. XRD patterns of the cross-sectioned area for the UPSD and BPSD composites fabricated by APADR process.

3. Results & discussion

3.1. Microstructures

Fig. 3 shows XRD patterns of the cross-sectioned area for the UPSD and BPSD composite fabricated by APADR process. In the UPSD composite, the diffraction peaks of Si_3N_4 were not detected, indicating the Si_3N_4 particles in the UPSD preform were completely transformed to AlN (and Si) within a minute of APADR. However, in the BPSD composite, the diffraction peaks of Si_3N_4 were detected because the larger Si_3N_4 particles (D_{50} = 14.8 μm) were partially transformed to AlN (and Si).

Fig. 4 shows (a) optical micrograph and (b) scanning electron micrograph of the UPSD composite. The microstructures of the composite exhibit co-continuous three dimensional network structures of Al and AlN. The thickness of the micro-channels was measured to be about 0.4 μm and 0.7 μm for Al (gray) and AlN (white), respectively [Fig. 4(b)]. In addition, a small amount of Si (black in Fig. 4(b)) with from 0.1 μm to 0.4 μm in diameter was precipitated during the solidification after displacement reaction. Indeed, the microstructure comprised of 55 vol%, 41 vol% and 4 vol% of AlN, Al and Si, respectively. The volume fraction of Si was small

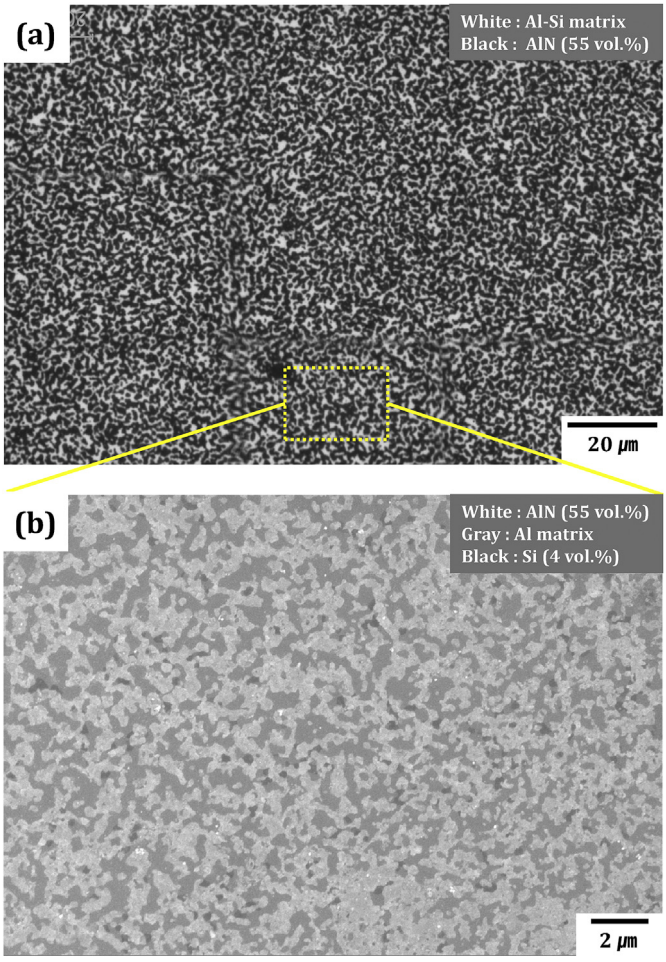

Fig. 4. (a) Optical micrograph and (b) scanning electron micrograph of the UPSD composite.

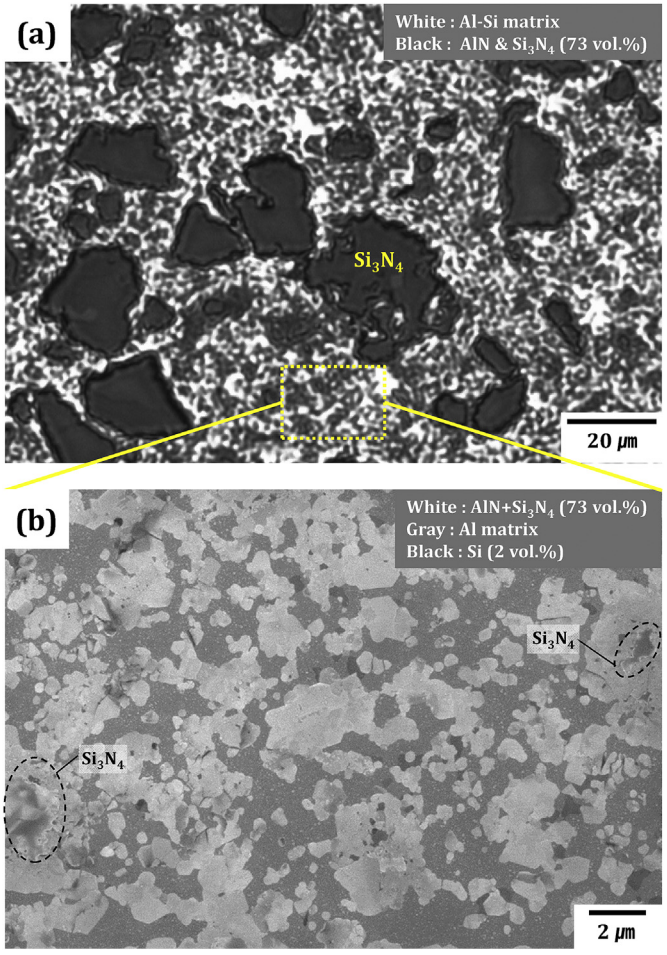

Fig. 5. (a) Optical micrograph and (b) scanning electron micrograph of the BPSD composite.

compared to AlN since Si diffused to the liquid reservoir (the Al ingot in Fig. 2) through the network structure. The volume fraction of AlN in the UPSD composite was about 10 vol% higher than the green density of the UPSD preform (45 vol%). One of the reasons is the formation of continuously interconnected AlN structure that leads to the reduction of porosity. Furthermore, the networking between the in-situ formed AlN was accelerated by their volumetric expansion during APADR process, which will be carefully discussed in Section 3.3.

Fig. 5 shows (a) optical micrograph and (b) scanning electron micrograph of the BPSD composite. The microstructure of the composite exhibits a quasi-continuous three dimensional network structures of Al and AlN with dispersed AlN surrounding Si_3N_4 particles (dark gray with black boundary in Fig. 5 (a)). A microstructural feature of the interspacing between dispersed Si_3N_4 particles is present in Fig. 5(b). In-situ formed AlN in Al matrix exhibits loosely interconnected structure, compared with those of UPSD composite. Thickness of the Al channel (gray) was about 1.0 μm, which is 2.5 time thicker than that of UPSD composite. The size of AlN (white) and precipitated Si (black) was in the range from 0.2 μm to 4.0 μm and from 0.4 μm to 1.0 μm, respectively. Volume fraction of Al, Si and nitrides (AlN and Si_3N_4) in the BPSD composite was confirmed to be 25 vol%, 2 vol% and 73 vol%, respectively. The nitride volume fraction in the BPSD composite was about 8 vol% higher than the green density of the BPSD preform (65 vol%). Interestingly, in case of Si_3N_4 particles with diameter larger than 4 μm, the unreacted Si_3N_4 remained inside the in-situ formed AlN layer [marked in Fig. 5(b)], which exhibited a rough and irregular edge compared with the smooth edge of the in-situ formed AlN. The reason of the confinement of the unreacted Si_3N_4 will be discussed in Section 3.3.

3.2. Pressureless infiltration

During APADR process, the Si_3N_4 preforms were infiltrated by molten Al without the aid of an external pressure. The infiltration was driven by capillary pressure:

$$\Delta P = -\frac{2\gamma_{lv}\cos\theta}{r_c} \quad (2)$$

where γ_{lv}, θ and r_c are liquid-vapor surface tension, contact angle between Si_3N_4 and liquid Al, and capillary radius of the preform, respectively. The surface tension of liquid Al varies according to the following equation [$\gamma_{lv} = (868–0.152 \times (T\text{-}T_m)) \times 10^{-3}$ [33]], and the contact angle of liquid Al on Si_3N_4 substrates decreases with increasing temperature [Fig. 1(b) [28,29]]. The capillary radius for a particulate preform can be estimated by Ref. [34]:

$$r_c = \frac{d_p(1-V_p)}{3\lambda V_p} \quad (3)$$

where d_p and V_p are the mean diameter and volume fraction of the particles in the preform and λ is geometry factor that is usually taken to be 1.4 [34]. The r_c for the UPSD preform (d_p = 0.7 and V_p = 0.45) and BPSD preform were estimated at 0.2 μm and 0.5 μm through a half of the thickness of Al channel in the UPSD and BPSD composites. Fig. 6 shows calculated capillary pressure for infiltration of the UPSD and BPSD preform with molten Al as a function of temperature. The contact angles less than 90° as shown in Fig. 1 (b) resulted in a negative value of capillary pressure at the elevated temperatures above 1273 K, leading to the pressureless infiltration of Al melt into the preforms. In the APADR process, with ultra-high temperature induced by arc plasma [32] and the exothermic heat of reaction in Equation (1), the negative value of capillary pressure could be larger than 1 MPa, which is a similar value of pressure applied for the infiltration of pure Al melt into several ceramic particulate preforms prepared from SiC, Al_2O_3 or B_4C (10–50 μm diameter and 50–60 vol% [8]). The negative value of capillary pressure was larger in the UPSD composite due to its smaller capillary radius, which implies that the infiltration of molten Al is more favorable for the UPSD preform. Thus, by newly developed APADR process, the infiltration of Al melt into the Si_3N_4 preform with smaller capillary radius (≤0.5 μm) and higher Si_3N_4 volume fraction (≤65 vol%) can be successfully carried out without an external pressure.

3.3. Volume nitridation mechanism

The core innovation of the APADR process is that it combines a simple pressureless infiltration with a thermodynamically favorable displacement reaction of Si_3N_4 and molten Al under arc-plasma induced ultra-high temperature. The fast volume displacement nitridation via the APADR resulted from improved wettability and enhanced diffusion of dissolved nitrogen. Thus, within a minute of APADR, the UPSD and BPSD composites containing nitrides over 50 vol% were fabricated by the infiltration of Al melt into Si_3N_4 particulate preforms with different particle size distributions. However, it should be noted that a bulk form of Si_3N_4 immersed in liquid Al creates a protective dense AlN layer that prevents further reaction [28]. The formation of the protective layer can be understood by considering the Pilling-Bedworth Ratio (PBR) between the reactant (Si_3N_4) and the product (AlN) as follows:

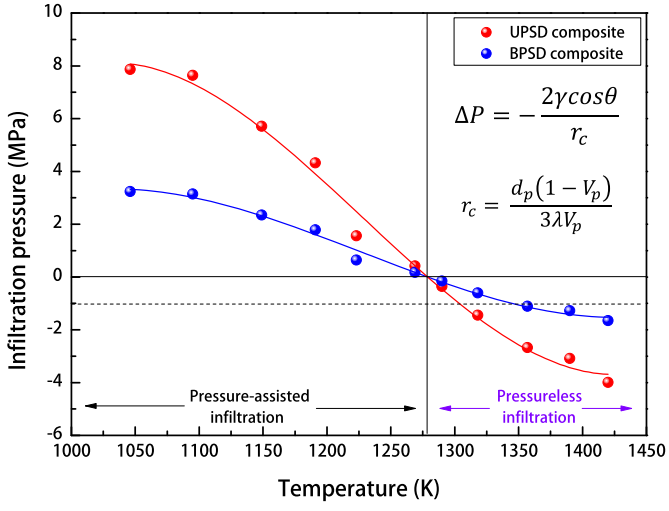

Fig. 6. Calculated capillary pressure for infiltration of the UPSD and BPSD preforms with molten Al as a function of temperature.

$$\text{PBR} = 4 \times \frac{molar\ volume\ of\ AlN}{molar\ volume\ Si_3N_4} = 4 \times \frac{w_{AlN}\rho_{Si3N4}}{w_{Si3N4}\rho_{AlN}} \quad (4)$$

where w and ρ are molar mass and density of the nitrides, respectively. The factor of 4 in Equation (4) arose from the stoichiometry of the reaction in Equation (1). Considering that w_{AlN}, w_{Si3N4}, ρ_{AlN} and ρ_{Si3N4} in Equation (4) are 40.98 g/mol, 140.3 g/mol, 3.26 g/cm^3 and 3.20 g/cm^3, respectively, the estimated PBR in the reaction was 1.15. The PBR of 1.15 indicates that the transformation entails an approximately 15% volumetric expansion, leading to the formation of protective AlN layer on the Si_3N_4 surface [22]. After APADR process, the UPSD and BPSD composites retained the initial diameter and shape of the UPSD and BPSD preforms; thus, the in-situ formation of AlN by the APADR process resulted in the significant increase of nitride volume fraction in the UPSD (55 vol%) and BPSD (73 vol%) composites compared with the green density of the UPSD (45 vol%) and BPSD (65 vol%) preforms. In the UPSD composite, the increase in AlN volume fraction was about 22%, which is higher than 15% estimated by the PBR calculation. In addition to the volumetric expansion of nitrides, the significant increase in the AlN volume fraction resulted from the formation of continuously interconnected AlN structure that reduces the porosity in the UPSD preform. And in the BPSD composite, the increase in volume fraction of nitrides was about 12%, which is lower than the UPSD composite. This is attributed to the addition of the relatively coarse Si_3N_4 particles that led to the formation of protective AlN layers on the coarse Si_3N_4 particles, leaving unreacted Si_3N_4 as shown in Fig. 5 (b). The thickness of the in-situ formed protective AlN layer is strongly dependent on the processing temperature as well as time. Within a minute of APADR process, the maximum thickness of the AlN layer formed on the Si_3N_4 surface was about 2 μm, which is thicker than 0.1 μm in the 6061Al–Si_3N_4 composites fabricated by pressure infiltration process at 1073 K for 1 h [25] or 1.0 μm at the interface between an Al drop and a Si_3N_4 substrate held at 1348 K for 1 h [28]. Thus, the critical diameter of Si_3N_4 particles for complete transformation to AlN by APADR process was about 4 μm. The mechanism for the formation of protective AlN layer and unreacted Si_3N_4 in the particles larger than the critical diameter was illustrated in Fig. 7. In particular, the displacement reaction of Si_3N_4 particles becomes prohibited as the particles are surrounded by the protective AlN layer, leaving unreacted Si_3N_4 and residual Al–Si melt inside the AlN layer; thus, the remaining Si_3N_4 exhibits rough and irregular edges according to the in-situ formed AlN.

Considering the critical diameter and PBR, a conversion ratio from Si_3N_4 to AlN in the BPSD composite can be estimated by the evaluation of the volume of AlN in-situ formed on the surface of the Si_3N_4 particles as follows.

$$1.15\left(V_{i,s} - V_{f,s}\right) = V_{f,p} - V_{f,s} \quad (5)$$

where 1.15 is the PBR calculated above, and $V_{i,s}$, $V_{f,s}$ and $V_{f,p}$ are the volume of a Si_3N_4 particle before the reaction, the volume of unreacted Si_3N_4 after the reaction and the total volume of the particle (Si_3N_4 with AlN layer) after the reaction, respectively. Assuming that the Si_3N_4 particles are spherical ($V_{i,s} = 4\pi r^3/3$) and the in-situ formed AlN covers the surface evenly for simple evaluation, the $V_{f,s}$ and $V_{f,p}$ were estimated as follows:

$$V_{f,s} = \frac{4\pi}{3}(r + \Delta r - 2)^3 \quad (6)$$

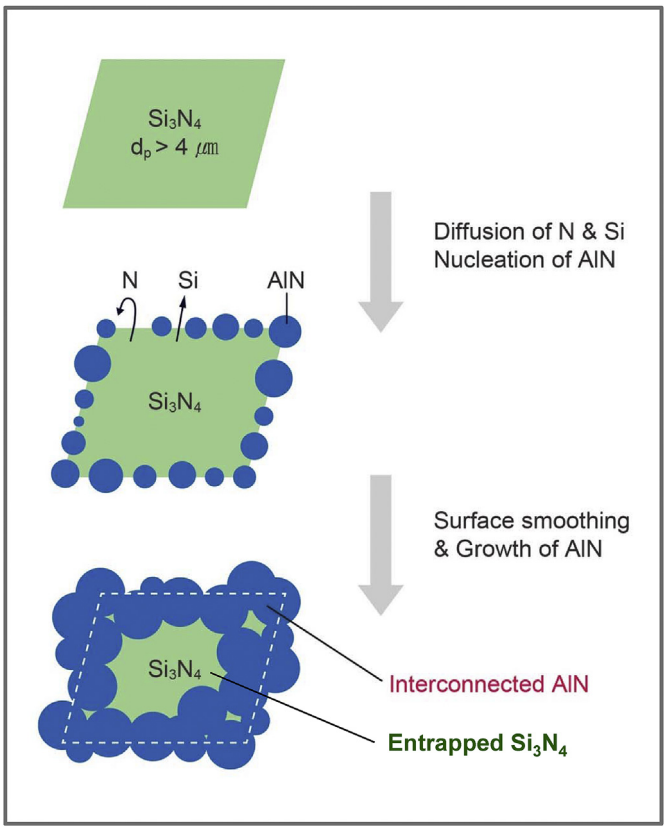

Fig. 7. Schematic diagrams showing the mechanism for the formation of unreacted Si_3N_4 during APADR process.

$$V_{f,p} = \frac{4\pi}{3}(r + \Delta r)^3 \quad (7)$$

where r is radius of particle in μm, Δr is an increase in the radius of particle due to the volumetric expansion by the displacement reaction and 2 is the critical thickness of the protective AlN layer. The volume of the in-situ formed AlN layer is the volumetric difference between the particle and unreacted Si_3N_4 after the reaction ($V_{f,p}-V_{f,s}$). Fig. 8 shows particle size distributions of Si_3N_4 powder in the UPSD and BPSD preforms and cumulative AlN fraction in the UPSD and BPSD composites. The UPSD composite exhibited a conversion ratio ~1, but the BPSD composite exhibited a conversion ratio ~0.75. With the conversion ratio, volume fraction of the in-situ formed AlN in the BPSD composite was estimated as 54.8 vol%. This estimation implies that the conversion ratio in APADR process is strongly dependent on the particle size distribution in the particulate preforms. Therefore, the total volume fraction of nitrides as well as microstructural features in nitride reinforced AMCs by APADR process can be manipulated by controlling the particle size distribution of a particulate preform.

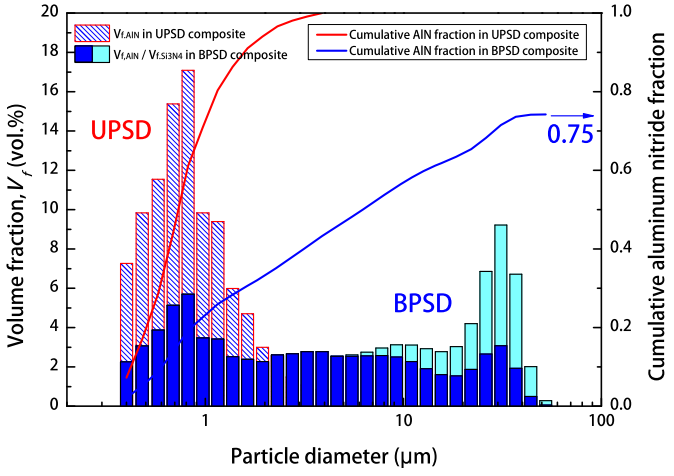

Fig. 8. Particle size distributions of Si_3N_4 powder in the UPSD and BPSD preforms and cumulative AlN fraction in the UPSD and BPSD composites.

3.4. Mechanical property

Fig. 9 shows flexural strength of the UPSD and BPSD composites versus the nitride volume fraction. The flexural strengths increased as volume fraction of nitrides increased, with the values of 268 MPa and 343 MPa for the UPSD and BPSD composites, respectively. The 21.4% increase in the strength compared with rule of mixtures between pure Al (70 MPa) and AlN (315 MPa) was measured for the UPSD composite, resulting from the presence of the precipitated Si (470 MPa [35]) in the Al channel and the formation of interconnected AlN structure that leads to the increase in residual internal stress and dislocation density in the Al channel [36]. However, the flexural strength of the BPSD composite was less than the value estimated by rule of mixture between Al and nitrides (471 MPa, estimated from the conversion ratio of 0.75) due to the formation of protective AlN layer accompanying volumetric expansion that builds up residual stresses, which is responsible for the low fracture resistance of the layer [26]. However, the BPSD composite showed a higher strength than monolithic AlN due to the formation of interconnected AlN structure and the presence of much stronger Si_3N_4 (941 MPa [37]) phase in the matrix. This suggests that AMCs containing both AlN and Si_3N_4 can be advantageous to improve the mechanical properties of AlN reinforced AMCs.

3.5. Thermal properties

Fig. 10 shows CTE of the UPSD and BPSD composites compared with that of various Al–AlN particulate composites and theoretically estimated values [10–14]. Compared to Turner's model

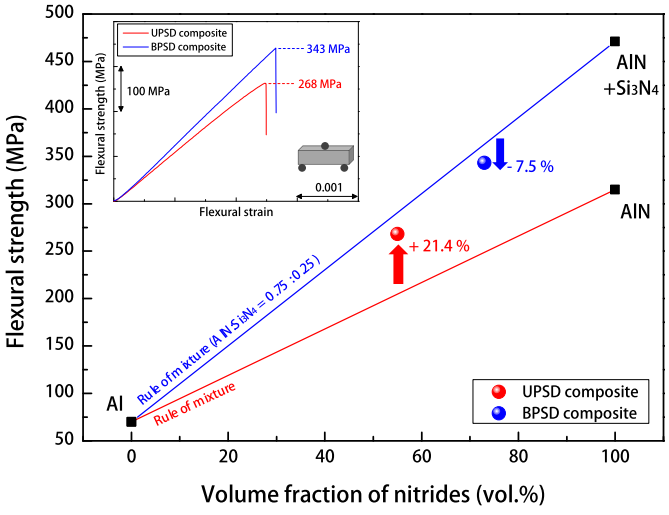

Fig. 9. Flexural strengths of the UPSD and BPSD composites with the lines obtained from the rule of mixtures between pure Al, AlN and Si_3N_4. The inset shows bending stress-strain curves for the UPSD and BPSD composites.

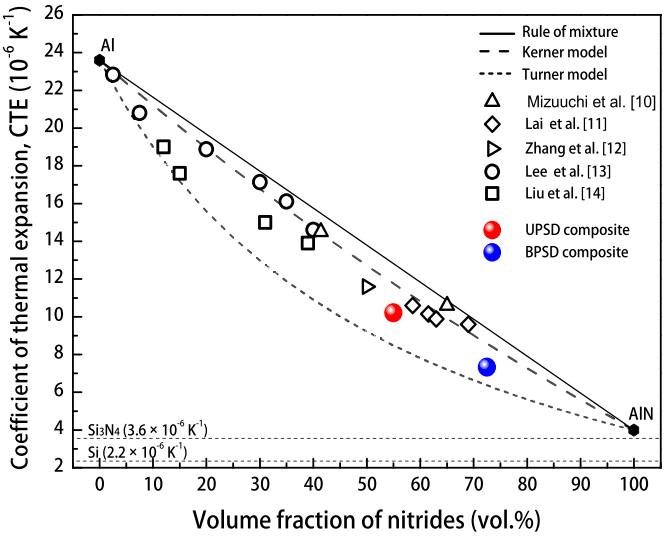

Fig. 10. CTE of the UPSD and BPSD composites compared with those of various Al–AlN particulate composites and theoretically estimated values by rule of mixture, Kerner model and Turner model [11–14].

assuming equilibrium of internal stress between particles and matrix [$\alpha_c=(\alpha_m V_m K_m+\alpha_p V_p K_p)/(V_m K_m + V_p K_p)$], CTE of the various particulate composites was well matched with Kerner's model assuming volumetric expansion of a spherical particle wet by matrix;

$$\alpha_c = \alpha_m V_m + \alpha_p V_p + V_p V_m (\alpha_p - \alpha_m) \times \frac{B_p - B_m}{V_m B_m + V_p B_p + 3B_p B_m / 4G_m} \quad (8)$$

where α, V, B and G represent CTE (23.6 × 10^{-6} K^{-1} for Al and 4.0 × 10^{-6} K^{-1} for AlN), volume fraction, bulk modulus (75.2 GPa for Al and 202 GPa for AlN) and shear modulus (26.2 GPa for Al and 126 GPa for AlN), respectively, and subscripts c, m and p refer to composites, matrix and particles, respectively. However, CTE of the present composites, with values of 10.2 × 10^{-6}/K and 7.33 × 10^{-6}/K for the UPSD and BPSD composites, respectively, was in between the Kerner model and Turner model that considers the effect of uniform hydrostatic stresses on adjacent phases [5]. The lower CTE of the present composites was attributed to the interconnected AlN structure that induces residual internal stress and large constraint in the Al matrix [38]. Moreover, the CTE of the present composites is also reduced by the presence of the precipitated Si (2.2 × 10^{-6}/K) and unreacted Si_3N_4 (3.6 × 10^{-6}/K). The CTE of the BPSD composite was 7.33 × 10^{-6}/K, which is the lowest among nitride reinforced AMCs ever reported [10–14] and is comparable to the CTE of GaAs (6 × 10^{-6}/K) or GaN (5.5 × 10^{-6}/K) used for high-power semiconductor devices [39]. It should be noted that the fabrication of AMCs with AlN more than 70 vol% requires an external pressure about 90–300 MPa [9,10] that is much larger than the capillary pressure estimated in APADR process (Fig. 6), resulting from the poor wettability of AlN by liquid Al [19]. Thus, the in-situ synthesis of AMCs with high volume fraction of nitrides by APADR process will be advantageous to produce materials needed to reduce CTE mismatch with the semiconductor that is crucial for the reliable heat dissipation in electronic devices with high-power density.

Fig. 11 shows linear expansion curves of the UPSD and BPSD composites compared with pure Al and in-situ formed Al-40 vol% AlN particulate composites [13] as a function of temperature. With an increase in the nitride volume fraction, the relative displacement

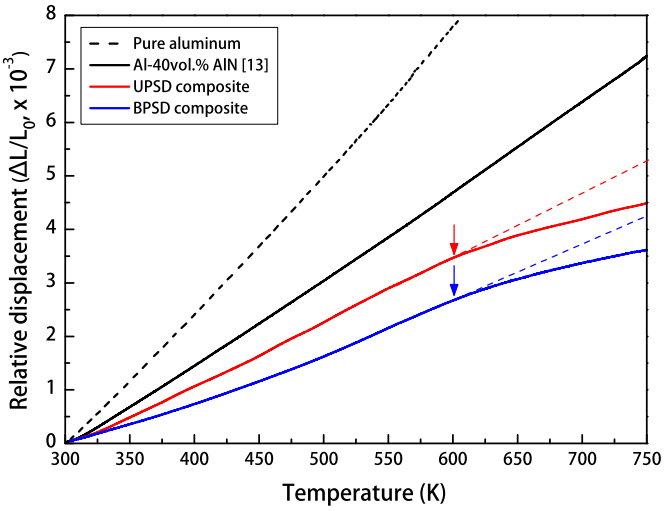

Fig. 11. Thermal expansion behaviors of the UPSD and BPSD composites as a function of temperature.

($\Delta L/L_0$) of the AMCs was reduced due to the low thermal expansivity of AlN and Si_3N_4. Compared to pure Al and the Al–AlN particulate composites, the present composites containing precipitated Si in the Al matrix showed a decrease in the slope of $\Delta L/L_0$ curves after 600 K, which is similar to thermal expansion behavior of SiC reinforced Al–Si alloy matrix composites [38,40]. The decrease in the slope is attributed to the increment of solid solubility of Si in Al with increasing temperature. Since the lattice parameter of Al decreases with an increase of dissolved Si in Al [41], the dissolution of the precipitated Si in the Al matrix reduces the thermal expansivity of the matrix at the elevated temperature. This suggests the opportunity for the use of the AMCs produced by the APADR of liquid Al and Si_3N_4 for unique structural applications requiring dimensional stability at elevated temperatures.

With respect to the thermal properties for the thermal management of electronics, a comparison with the other AMCs reinforced with in-situ formed Al_2O_3 [21] and AlN [13–15] is shown on the plot of TC versus CTE in Fig. 12. The in-situ formed AMCs showed lower TC compared with the pure components (230 W/mK for Al, 200 W/mK for AlN, 30 W/mK for Al_2O_3). The low TC is

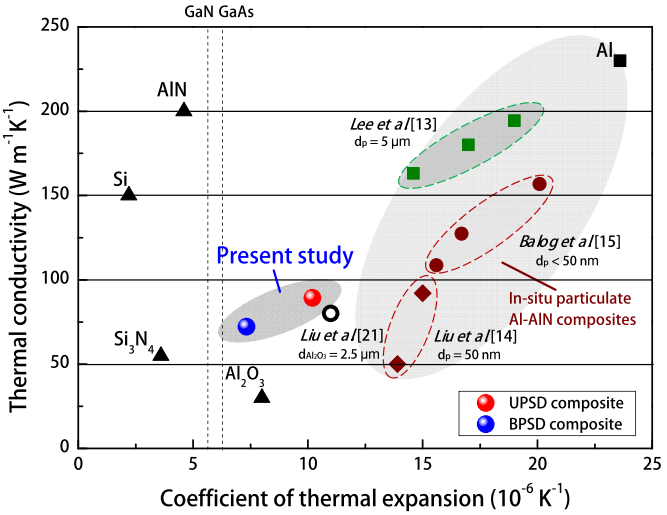

Fig. 12. Correlation between TC and CTE of the UPSD and BPSD composites compared with various in-situ AMCs reinforced with Al_2O_3 [21] and AlN [13–15,21].

attributed to a thermal barrier resistance at the interface between the components [42], which can be evaluated by H-J model as follows:

$$K_c = K_m \frac{\left[2\left(\frac{K_p}{K_m} - \frac{K_p}{r_p h} - 1\right)V_p + \frac{K_p}{K_m} + \frac{K_p}{r_p h} + 2\right]}{\left[\left(1 - \frac{K_p}{K_m} + \frac{K_p}{r_p h}\right)V_p + \frac{K_p}{K_m} + \frac{K_p}{r_p h} + 2\right]} \quad (9)$$

where K, r and h represent TC, radius of particulates and interfacial thermal conductance, respectively. The model represents that a decrease in reinforcement size results in the decrease in TC due to an increase in interfacial area between the components. This explains a significant decrease in TC for the Al–AlN nanocomposites ($d_p \leq 50$ nm) produced by plasma evaporation [14] or surface nitridation at 833 K [15]. The size of in-situ formed AlN in the present composites is larger than several hundred nanometers, which results in a moderate TC compared with the nanocomposites [14,15] and microcomposites produced by arc plasma-induced nitridation ($d_p \sim 5$ μm) [13]. TC of the UPSD composite (89.4 W/mK) is comparable to the TC of a particulate composite which contains 55 vol% AlN with particle size of 0.7 μm and shows interfacial thermal conductance of 3.2×10^7 W/m^{2}K that is estimated by the H-J model (Equation (9)). This implies that the UPSD composite fabricated by APADR process exhibits high interfacial thermal conductance due to the strong interfacial bonding induced by exothermic heat of the displacement reaction [Equation (1)] and arc plasma-induced ultra-high temperature [13,32] that improves wettability of AlN by liquid Al [19]. The BPSD composite (72.1 W/mK) exhibited a slight decrease in TC compared with the UPSD composite despite the presence of unreacted Si_3N_4 (55 W/mK [37]). This results from the formation of thermally conductive AlN protective layer on the surface of the coarse Si_3N_4 particles and the increase in the thickness of Al channels (1.0 μm) compared with the UPSD composite (0.4 μm), which leads to a decrease in total interfacial area.

The thermal properties of interconnected Al–Al_2O_3 composite, produced by the displacement reaction of liquid Al and SiO_2, were shown in Fig. 12 (11×10^{-6}/K for CTE and 80 W/mK for TC [21], marked as an open circle). Compared with this Al–Al_2O_3 composite containing more and larger reinforcement (64 vol% and 2.5 μm) than the UPSD composites (55 vol% 0.7 μm), the present composites showed a more attractive combination of TC and CTE since thermal properties of AlN (200 W/mK and 4.4×10^{-6}/K) are better than that of Al_2O_3 (30 W/mK and 8.0×10^{-6}/K). Consequently, it can be understood that AMCs with high AlN volume fraction (≥50 vol%) by APADR process exhibited a unique combination of relatively high TC and much reduced CTE with high interfacial thermal conductance due to the strong interfacial bonding.

4. Conclusions

Our study highlights the in-situ synthesis of co-continuous Al–AlN composites with attractive mechanical and thermal properties via newly developed APADR process. The fast volume displacement nitridation via APADR resulted from a unique combination between a simple pressureless infiltration and a thermodynamically favorable displacement reaction of Si_3N_4 and molten Al under arc-plasma induced ultra-high temperature. The total volume fraction of nitrides as well as microstructural features in nitride reinforced AMCs by APADR process can be manipulated by controlling the particle size distribution of a preform. Thus, within a minute of APADR, the UPSD composite (55 vol% AlN) and BPSD composite (73 vol% 0.75AlN-0.25Si_3N_4) were successfully fabricated by the infiltration of Al melt into the USPD and BPSD performs with smaller capillary radius (≤0.5 μm) and higher Si_3N_4 volume fraction (≤65 vol%). The resultant composites exhibited co-continuous three-dimensional network structures with strong interfacial bonding and high interfacial thermal conductance, which resulted in a unique combination of relatively high flexural strength and high TC (268 MPa and 89.4 W/mK for UPSD composite, 343 MPa and 71.2 W/mK for BPSD composite). In particular, the BPSD composite exhibited low CTE (7.33×10^{-6}/K), close to those of GaAs or GaN, which will be advantageous to produce materials needed to reduce CTE mismatch with the semiconductor that is crucial for reliable heat dissipation in electronic devices with high-power density. These results give us a guideline on how to fabricate in-situ co-continuous Al–AlN composites with tailored properties via APADR process for heat spreader applications.

Acknowledgement

This work was supported by the National Research Foundation of Korea (NRF) grant funded by the Korean government (Ministry of Science, ICT and Future Planning) (No. 2014K1A3A1A20034841 & 2014M1A7A1A01030139). ESPark also benefited from the Center for Iron and Steel Research and Engineering Research Institute at Seoul National University.

References

[1] D. Miracle, Metal matrix composites–from science to technological significance, Compos. Sci. Technol. 65 (15) (2005) 2526–2540.
[2] C. Zweben, Advances in composite materials for thermal management in electronic packaging, JOM 50 (6) (1998) 47–51.
[3] S.C. Tjong, Z. Ma, Microstructural and mechanical characteristics of in situ metal matrix composites, Mater. Sci. Eng. R Rep. 29 (3) (2000) 49–113.
[4] M. Koczak, M.K. Premkumar, Emerging technologies for the in-situ production of MMCs, JOM 45 (1) (1993) 44–48.
[5] K.K. Chawla, Metal Matrix Composites, Wiley Online Library, 2006.
[6] B. Prabhu, C. Suryanarayana, L. An, R. Vaidyanathan, Synthesis and characterization of high volume fraction Al–Al 2 O 3 nanocomposite powders by high-energy milling, Mater. Sci. Eng. A 425 (1) (2006) 192–200.
[7] A. Arsha, E. Jayakumar, T. Rajan, V. Antony, B. Pai, Design and fabrication of functionally graded in-situ aluminium composites for automotive pistons, Mater. Des. 88 (2015) 1201–1209.
[8] C. Garcia-Cordovilla, E. Louis, J. Narciso, Pressure infiltration of packed ceramic particulates by liquid metals, Acta Mater. 47 (18) (1999) 4461–4479.
[9] B. Dun, X. Jia, C. Jia, K. Chu, Thermal conductivity behavior of SPS consolidated AlN/Al composites for thermal management applications, Rare Met. 30 (2) (2011) 189–194.
[10] K. Mizuuchi, K. Inoue, Y. Agari, T. Nagaoka, M. Sugioka, M. Tanaka, T. Takeuchi, J.-I. Tani, M. Kawahara, Y. Makino, Processing and thermal properties of Al/AlN composites in continuous solid–liquid co-existent state by spark plasma sintering, Compos. B Eng. 43 (3) (2012) 1557–1563.
[11] S.-W. Lai, D. Chung, Superior high-temperature resistance of aluminium nitride particle-reinforced aluminium compared to silicon carbide or alumina particle-reinforced aluminium, J. Mater. Sci. 29 (23) (1994) 6181–6198.
[12] Q. Zhang, G. Chen, G. Wu, Z. Xiu, B. Luan, Property characteristics of a AlNp/Al composite fabricated by squeeze casting technology, Mater. Lett. 57 (8) (2003) 1453–1458.
[13] J.I. Lee, E.S. Park, In situ synthesis of cold-rollable aluminum–aluminum nitride composites via arc plasma-induced accelerated volume nitridation, J. Mater. Res. (2016) 1–10.
[14] Y.Q. Liu, H. Cong, H. Cheng, Thermal properties of nanocrystalline Al composites reinforced by AlN nanoparticles, J. Mater. Res. 24 (1) (2009) 24–31.
[15] M. Balog, P. Yu, M. Qian, M. Behulova, P. Svec, R. Cicka, Nanoscaled Al–AlN composites consolidated by equal channel angular pressing (ECAP) of partially in situ nitrided Al powder, Mater. Sci. Eng. A 562 (2013) 190–195.
[16] H. Scholz, P. Greil, Nitridation reactions of molten Al-(Mg, Si) alloys, J. Mater. Sci. 26 (3) (1991) 669–677.
[17] C. Borgonovo, D. Apelian, Processing of Lightweight Metal Matrix Composites via in situ Gas/Liquid Reaction, Materials Science Forum, Trans Tech Publ, 2011, pp. 115–123.
[18] Q. Zheng, B. Wu, R.G. Reddy, In-situ processing of Al alloy composites, Adv. Eng. Mater. 5 (3) (2003) 167–172.
[19] C. Toy, W. Scott, Wetting and spreading of molten aluminium against AlN surfaces, J. Mater. Sci. 32 (12) (1997) 3243–3248.
[20] M. Breslin, J. Ringnalda, L. Xu, M. Fuller, J. Seeger, G. Daehn, T. Otani, H. Fraser, Processing, microstructure, and properties of co-continuous alumina-aluminum composites, Mater. Sci. Eng. A 195 (1995) 113–119.
[21] W. Liu, U. Köster, Microstructures and properties of interpenetrating alumina/aluminium composites made by reaction of SiO 2 glass preforms with molten

aluminium, Mater. Sci. Eng. A 210 (1) (1996) 1–7.
[22] E. Saiz, A.P. Tomsia, Kinetics of metal-ceramic composite formation by reactive penetration of silicates with molten aluminum, J. Am. Ceram. Soc. 81 (9) (1998) 2381–2393.
[23] J. Zhang, J.-M. Lee, Y.-H. Cho, S.-H. Kim, H. Yu, Fabrication of aluminum matrix composites by quick spontaneous infiltration process through combustion reaction of Al–Ti–B 4 C–CuO powder mixtures in molten aluminum, Scripta Mater. 69 (1) (2013) 45–48.
[24] J.F. Elliott, M. Gleiser, Thermochemistry for Steelmaking, Addison-Wesley, Reading, 1963, p. 160.
[25] K.B. Lee, H. Kwon, Fabrication and characteristics of AA6061/Si3N4p composite by the pressureless infiltration technique, Metall. Mater. Trans. 30 (11) (1999) 2999–3007.
[26] Y. Lu, J. Yang, W. Lu, R. Liu, G. Qiao, C. Bao, The mechanical properties of co-continuous Si 3 N 4/Al composites manufactured by squeeze casting, Mater. Sci. Eng. A 527 (23) (2010) 6289–6299.
[27] F. Akhtar, S.-J. Guo, Development of Si3N4/Al composite by pressureless melt infiltration, Trans. Nonferrous Metals Soc. China 16 (3) (2006) 629–632.
[28] L. Mouradoff, A. Lachau-Durand, J. Desmaison, J. Labbe, O. Grisot, R. Rezakhanlou, Study of the interaction between liquid aluminum and silicon nitride, J. Eur. Ceram. Soc. 13 (4) (1994) 323–328.
[29] S.-R. Wang, Y.-Z. Wang, Y. Wang, H.-R. Geng, Q. Chi, Microstructure and infiltration kinetics of Si3N4/Al–Mg composites fabricated by pressureless infiltration, J. Mater. Sci. 42 (18) (2007) 7812–7818.
[30] C.Y. Ho, M. Ackerman, K. Wu, S. Oh, T. Havill, Thermal conductivity of ten selected binary alloy systems, J. Phys. Chem. Ref. Data 7 (3) (1978) 959–1178.
[31] J. Molina, R. Saravanan, R. Arpón, C. Garcıa-Cordovilla, E. Louis, J. Narciso, Pressure infiltration of liquid aluminium into packed SiC particulate with a bimodal size distribution, Acta Mater. 50 (2) (2002) 247–257.
[32] K. Etemadi, Formation of aluminum nitrides in thermal plasmas, Plasma Chem. Plasma Process. 11 (1) (1991) 41–56.
[33] J.E. Hatch, A. Association, Aluminum: Properties and Physical Metallurgy, ASM International, 1984.
[34] M. Pech-Canul, R. Katz, M. Makhlouf, Optimum conditions for pressureless infiltration of SiC p preforms by aluminum alloys, J. Mater. Process. Technol. 108 (1) (2000) 68–77.
[35] T. Namazu, Y. Isono, T. Tanaka, Evaluation of size effect on mechanical properties of single crystal silicon by nanoscale bending test using AFM, J. Microelectromech. Syst. 9 (4) (2000) 450–459.
[36] R. Arsenault, L. Wang, C. Feng, Strengthening of composites due to microstructural changes in the matrix, Acta Metall. Mater. 39 (1) (1991) 47–57.
[37] M. Fukuhara, K. Fukazawa, A. Fukawa, Physical properties and cutting performance of silicon nitride ceramic, Wear 102 (3) (1985) 195–210.
[38] T. Huber, H.-P. Degischer, G. Lefranc, T. Schmitt, Thermal expansion studies on aluminium-matrix composites with different reinforcement architecture of SiC particles, Compos. Sci. Technol. 66 (13) (2006) 2206–2217.
[39] R.S. Pengelly, S.M. Wood, J.W. Milligan, S.T. Sheppard, W.L. Pribble, A review of GaN on SiC high electron-mobility power transistors and MMICs, IEEE Trans. Microw. Theor. Tech. 60 (6) (2012) 1764–1783.
[40] Z. Wei, P. Ma, H. Wang, C. Zou, S. Scudino, K. Song, K.G. Prashanth, W. Jiang, J. Eckert, The thermal expansion behaviour of SiC p/Al–20Si composites solidified under high pressures, Mater. Des. 65 (2015) 387–394.
[41] T. Hahn, R. Armstrong, Internal stress and solid solubility effects on the thermal expansivity of Al-Si eutectic alloys, Int. J. Thermophys. 9 (2) (1988) 179–193.
[42] D.P.H. Hasselman, L.F. Johnson, Effective thermal conductivity of composites with interfacial thermal barrier resistance, J. Compos. Mater. 21 (6) (1987) 508–515.